Asymmetrical two-dimensional magnetic lattices for ultracold atoms

A. Abdelrahman,* M. Vasiliev, and K. Alameh
Electron Science Research Institute, Edith Cowan University, 270 Joondalup Drive, Joondalup, Western Australia 6027, Australia

P. Hannaford†
Centre for Atom Optics and Ultrafast Spectroscopy, and ARC Centre of Excellence for Quantum Atom Optics, Swinburne University of Technology, Melbourne 3122, Australia

(Received 18 December 2009; published 19 July 2010)

A simple method for implementing an asymmetrical two-dimensional magnetic lattice is proposed. The asymmetrical two-dimensional magnetic lattice is created by periodically distributing nonzero magnetic minima across the surface of a magnetic thin film, where the magnetic patterns are formed by milling $n \times n$ square holes on the surface of the film. The method is proposed for trapping and confining quantum degenerate gases, such as Bose-Einstein condensates and ultracold Fermi gases, prepared in low-magnetic-field-seeking states. Analytical expressions and numerical simulation results of the magnetic local minima are shown where we analyze the effect of changing the magnetic lattice parameters, such as the separation of the holes, the hole size, and external bias magnetic fields, to maintain and locate the nonzero local minima at a suitable distance above the film surface to avoid the effect of Majorana spin flips and the Casimir-Polder potential.

DOI: 10.1103/PhysRevA.82.012320 PACS number(s): 03.67.Ac, 67.85.Hj, 52.55.Jd

I. INTRODUCTION

The field of quantum degenerate gases in periodically distributed microscopic potentials has gained considerable attention over the last decade; it is being explored to unlock the answers to various interesting fundamental questions in physics. In particular, the field of trapped ultracold atoms in optical confining fields, that is, optical lattices [1], has achieved remarkable results in the simulation of condensed-matter systems. Optical lattices are recognized for their ability to coherently transfer cold atoms, via spin-dependent transport, between the lattice sites [2]. Such coherent manipulation has made it possible, using trapped low-dimensional quantum gases [3,4], to establish realizable analogies with condensed-matter systems [5]. As an example, the Mott insulator to superfluid transition has been observed using optically trapped Bose-Einstein condensates [6] and, more interestingly, the transition has also been realized using optically trapped ultracold fermionic gases [7], as well as the observation of the Fermi surfaces [8].

In the context of quantum processors using trapped ultracold atoms, it is crucial to satisfy the scalability criterion in order to process quantum information [9]; optical lattices are thought to provide scalable quantum systems where, remarkably, they have allowed large-scale quantum entanglement [10,11], pointing to the possibility of using such ensembles to serve as quantum processing units.

Integrating ultracold atoms with magnetic microstructures [12] and the creation of Bose-Einstein condensates on an atom chip [13–15] have triggered an alternative approach to optical lattices. To realize a magnetic lattice, periodically distributed nonzero magnetic-field local minima are created by fabricating microscopic patterns on the surface of permanent magnetic materials [16–18] or by using current carrying microwires [19]. Magnetic lattices created using permanent magnetic films have very low technical noise and relatively high magnetic-field gradients with no resistive heating and offer a highly stable trapping environment for ultracold atoms. It is also possible to construct magnetic lattices in one- or two-dimensional configurations where the flexibility of the design and current state-of-the art fabrication technologies allow the implementation of arbitrary trap geometries and scalable lattice spacing [20,21].

Only atoms prepared in low-field-seeking states are attracted to, and trapped in, the distributed confining magnetic potentials above the surface, allowing magnetic-state selectivity as a characteristic identity of magnetic lattices. This provides a remarkable opportunity to employ on-chip detection and manipulation techniques [22] such as applying radio-frequency fields for on-site atomic manipulation [11], evaporative cooling, and spectroscopy [23].

One-dimensional magnetic lattices have been used as magnetic mirrors to reflect atoms in low field-seeking states [24–27] and, in recent experiments, radial trap frequencies of up to 90 kHz have been measured for ^{87}Rb atoms trapped at a distance of ~ 5 μm below the surface of a one-dimensional permanent magnetic lattice [18]. Trapped gases with temperatures of $T = 2.0 \pm 0.3$ μK have been observed in a permanent two-dimensional (2D) magnetic microstructure [23] and coherence times of the order of 1 s have been recorded for cold ^{87}Rb atoms trapped in two different hyperfine states on an atom chip [12,28]. A Raman focused laser may be used to selectively drive the cold atoms into highly excited Rydberg states, as proposed in [23], which can also lead to the dipole blockade mechanism [29,30], exhibiting a single Rydberg excitation per lattice site.

This has attracted the attention to examine qubit formation and entanglement in magnetic lattices. The internal hyperfine, or Zeeman, magnetic states of the trapped cold atoms can be used to encode the qubit states $|0\rangle$ and $|1\rangle$, where recently a superposition of two hyperfine states with a long coherence lifetime has been demonstrated [28], indicating the possibility

*a.abdelrahman@ecu.edu.au
†Phannaford@swin.edu.au

of constructing quantum gates with a lifetime longer than the gate operation time [31,32]. This as well suggests that magnetic lattices are promising candidates for a scalable quantum processing unit.

In this article, we present a simple method for creating 2D magnetic lattice to microscopically confine ultracold quantum degenerate gases. The proposed magnetic lattice shows an asymmetrical feature which can be used to simulate condensed-matter systems [33] where the asymmetrical effect introduces a tilt in the magnetic potential similar to the potential tilt in optical lattices [34,35]. It also introduces what we call the *gravitational offset* along the gravitational-field axis [36].

In Sec. II we describe the magnetic lattice structure and in Sec. III we describe the characteristic parameters and their effect in maintaining a magnetic lattice with suitable trapping sites.

II. MAGNETIC-LATTICE STRUCTURE

The proposed structure of the generated magnetic lattice is realized by milling an $n \times n$ array of square holes of width α_h, separated by α_s, in a magneto-optic thin film of thickness τ deposited onto a suitable substrate, where n represents the number of holes, as illustrated in Figs. 1(a) and 1(b). The depths of all holes are equal and the holes extend through the thin film down to the surface of the substrate. The presence of the holes results in a magnetic-field distribution having local minima located at effective z distances, $d_{\min}$, from the top of the holes. The structure generates periodically distributed 2D magnetic-field minima above the surface of the thin film in which the distribution creates a magnetic lattice with $n \times n$ sites or potential wells. The magnetic device is in its remanently magnetized state with magnetization M_z perpendicular to the surface plane. We note that this structure is a special case of the class of magnetic lattices proposed in [16,18], with $t_1 = t_2$ and $t_3 = 0$.

We assume an infinite lattice with hole widths equal to their separations, that is, $\alpha_h = \alpha_s \equiv \alpha$, to simplify the mathematical derivation. The spatial magnetic-field components B_x, B_y, and B_z can be written as a combination of a field decaying with distance from the surface of the traps in the z direction and a periodically distributed magnetic field in the x-y plane produced by the magnetic induction, $B_0 = \mu_0 M_z/\pi$, at the surface of the magnetized thin film. We define a surface reference magnetic field $B_{\text{ref}} = B_0(1 - e^{-\beta\tau})$, where $\beta = \pi/\alpha$, and a plane of symmetry is assumed at $z = 0$. We include in the analysis external magnetic-bias-field components, $B_{x\,\text{bias}}$, $B_{y\,\text{bias}}$, and $B_{z\,\text{bias}}$, which can be produced by the microfabricated configuration. The analytical expressions that describe the nonzero local minima are derived and simplified to the following set of equations:

$$B_x = B_{\text{ref}} \sin(\beta x) e^{-\beta[z-\tau]} - \frac{B_{\text{ref}}}{3} \sin(3\beta x) e^{-3\beta[z-\tau]} + \cdots + B_{x\,\text{bias}}, \quad (1)$$

$$B_y = B_{\text{ref}} \sin(\beta y) e^{-\beta[z-\tau]} - \frac{B_{\text{ref}}}{3} \sin(3\beta y) e^{-3\beta[z-\tau]} + \cdots + B_{y\,\text{bias}}, \quad (2)$$

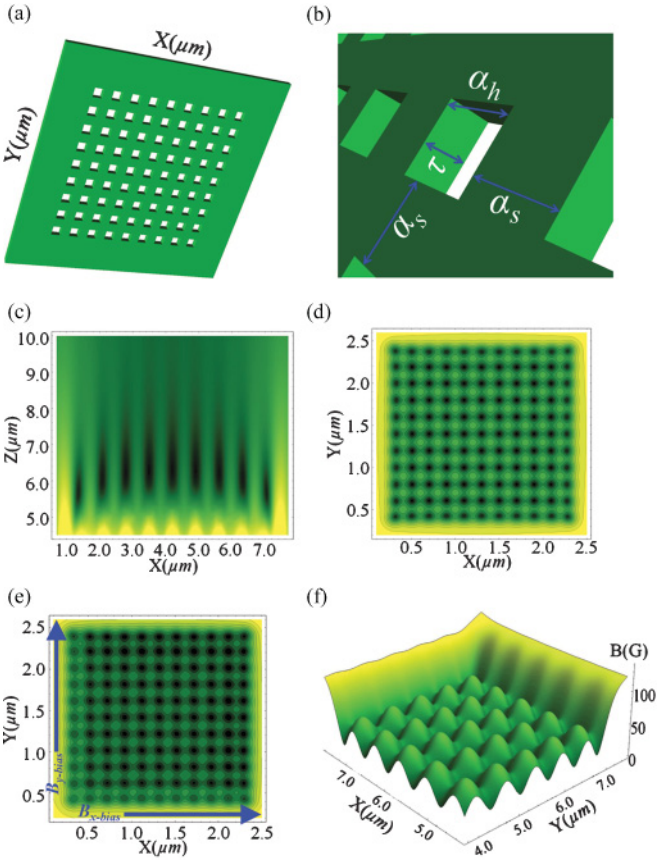

FIG. 1. (Color online) (a) Schematic representation of a magnetic lattice. (b) The magnetic lattice parameters are specified by the hole size $\alpha_h \times \alpha_h$, the separation between the holes α_s, and the magnetic film thickness τ. (c) Magnetic density plot of the simulated finite magnetic lattice sites in the z-x plane across the center of the lattice. The traps are located at an effective z distance, $d_{\min}$, above the holes. (d,e) Contour plots of the distributed lattice sites across the x-y plane without (d) and (e) with application of bias fields of $B_{x\,\text{bias}} = B_{y\,\text{bias}} =$ 10 G. (f) 3D plot of the magnetic field of the distributed sites across the x-y plane at $d_{\min}$. The field is displayed from the center sites to the edge sites. Simulation input parameters: $\alpha_s = \alpha_h = 1$ μm, $M_z =$ 3 kG, and $\tau = 2$ μm.

$$B_z = B_{\text{ref}}[\cos(\beta x) + \cos(\beta y)] e^{-\beta[z-\tau]} - \frac{B_{\text{ref}}}{3}[\cos(3\beta x) + \cos(3\beta y)] e^{-3\beta[z-\tau]} \cdots + B_{z\,\text{bias}}. \quad (3)$$

We neglect the higher-order terms in the preceding equations because atoms prepared in low-field-seeking states are trapped in local magnetic minima located at $d_{\min} > \alpha/2\pi$. Thus, Eqs. (1)–(3) reduce to the following:

$$B_x = B_0(1 - e^{-\beta\tau})\, e^{-\beta[z-\tau]} \sin(\beta x) + B_{x\,\text{bias}}, \quad (4)$$

$$B_y = B_0(1 - e^{-\beta\tau})\, e^{-\beta[z-\tau]} \sin(\beta y) + B_{y\,\text{bias}}, \quad (5)$$

$$B_z = B_0(1 - e^{-\beta\tau})\, e^{-\beta[z-\tau]}[\cos(\beta x) + \cos(\beta y)] + B_{z\,\text{bias}}. \quad (6)$$

The magnitude B of the magnetic field above the film surface can be written, using Eqs. (4)–(6), as

$$\begin{aligned} B(x,y,z) = \big(&B_{x\,\mathrm{bias}}^2 + B_{y\,\mathrm{bias}}^2 + B_{z\,\mathrm{bias}}^2 \\ &+ 2B_{\mathrm{ref}}^2[1+\cos(\beta x)\cos(\beta y)]e^{-2\beta[z-\tau]} \\ &+ 2B_{\mathrm{ref}}e^{-\beta[z-\tau]}\{\sin(\beta x)B_{x\,\mathrm{bias}} + \sin(\beta y)B_{y\,\mathrm{bias}} \\ &+ [\cos(\beta x)+\cos(\beta y)]B_{z\,\mathrm{bias}}\}\big)^{1/2}. \end{aligned} \tag{7}$$

The distribution of the nonzero local minima is periodic, and the magnetic-field minima, $B_{\min}$, are located at points defined by the coordinates $(x_{\min}, y_{\min}, d_{\min})$. The location of the minima along the x, y, and z axes for an infinite magnetic lattice can be written as

$$x_{\min} = n_x\alpha, \quad n_x = 0, \pm 1, \pm 2, \ldots, \tag{8}$$

$$y_{\min} = n_y\alpha, \quad n_y = 0, \pm 1, \pm 2, \ldots, \tag{9}$$

$$d_{\min} \approx \frac{\alpha}{\pi}\ln(B_{\mathrm{ref}}). \tag{10}$$

The parameters $d_{\min}$ and $B_{\min}$ can significantly influence the lifetime of the trapped cold atoms, making it crucial to initially choose suitable values of $B_{\min}$ and $d_{\min}$ when microfabricating the magnetic lattice structure.

Each individual potential well, that is, lattice site, is confined through magnetic barriers $\Delta B(\mathbf{x})$ in which their heights are determined by

$$\Delta B(\mathbf{x}) = |B_{\max}(\mathbf{x})| - |B_{\min}(\mathbf{x})|, \quad \mathbf{x} \equiv (x,y,z). \tag{11}$$

The magnetic fields around the local minima have symmetrically distributed gradients across the x-y plane. The curvatures along the x and y axes are given by

$$\begin{aligned} \frac{\partial^2 B}{\partial x^2} = -\beta^2 e^{\beta[z-\tau]}B_{\mathrm{ref}}\Bigg\{&\frac{\cos(\beta x)\cos(\beta y)}{\sqrt{2+2\cos(\beta x)\cos(\beta y)}} \\ &+ \frac{\cos^2(\beta y)\sin^2(\beta x)}{[2+2\cos(\beta x)\cos(\beta y)]^{3/2}}\Bigg\}, \end{aligned} \tag{12}$$

$$\begin{aligned} \frac{\partial^2 B}{\partial y^2} = -\beta^2 e^{\beta[z-\tau]}B_{\mathrm{ref}}\Bigg\{&\frac{\cos(\beta x)\cos(\beta y)}{\sqrt{2+2\cos(\beta x)\cos(\beta y)}} \\ &+ \frac{\cos^2(\beta x)\sin^2(\beta y)}{[2+2\cos(\beta x)\cos(\beta y)]^{3/2}}\Bigg\}. \end{aligned} \tag{13}$$

Due to the x-y symmetry for an unbiased magnetic lattice, we find that at the centers of the traps $\frac{\partial^2 B}{\partial x^2} = \frac{\partial^2 B}{\partial y^2}$ holds. The curvature of the trapping magnetic field at each individual site is of particular importance when loading the ultracold atoms into the magnetic lattice. Lattice sites with a steeper gradient may develop a destructive Majorana spin-flip process. The loading procedure in this type of magnetic lattice is reported elsewhere [17].

The curvatures along the confining directions determine the trapping frequencies, $\nu_{x,y,z}$, which depend on the Zeeman sublevels. For the case of a harmonic potential they are given by

$$\nu_k = \frac{\beta}{2\pi}\sqrt{\mu_B g_F m_F \frac{\partial^2 B}{\partial k^2}}, \quad k = x,y,z, \tag{14}$$

and $\nu_z = \sqrt{\nu_x^2 + \nu_y^2}$, where g_F is the Landé g-factor, μ_B is the Bohr magneton, and m_F is the magnetic quantum number of the hyperfine state. The nonzero local minimum values determine the depth of the harmonic potential traps, where, for an external trapping magnetic field $B \ll \frac{\hbar\Delta\eta}{\mu_B g_F m_F}$, in which the hyperfine splitting $\Delta\eta$ is larger than the Zeeman splitting, the depth Λ_{depth} of an individual trap can be expressed as

$$\Lambda_{\mathrm{depth}}(\mathbf{x}) = \frac{\mu_B g_F m_F}{k_B}\Delta B(\mathbf{x}) \tag{15}$$

where k_B is the Boltzmann constant. The magnetic potential is defined as $V(\mathbf{x}) = \mu_B g_F m_F B$, and the potential barrier heights in the k direction are given by

$$\begin{aligned} \Delta V^k(\mathbf{x}) &= \Delta V^k(\mathbf{x})_{\max} - \Delta V^k(\mathbf{x})_{\min} \\ &= \mu_B g_F m_F \Delta B^k(\mathbf{x}) = k_B \Lambda_{\mathrm{depth}}(\mathbf{x}). \end{aligned} \tag{16}$$

For ^{87}Rb atoms in a low-magnetic-field-seeking state with $F = 2$ and $m_F = +2$, the potential barrier heights along the x, y, and z axes are $\Delta V^x \approx 184$ μK, $\Delta V^y \approx 186$ μK, and $\Delta V^z \approx 122$ μK, respectively, where $\Delta B^x = 2.74$ G, $\Delta B^x = 2.78$ G, and $\Delta B^z = 1.83$ G. The lattice parameters are $\alpha_h = \alpha_s = 3.5$ μm, $\tau = 2$ μm, $M_z = 3.80$ kG, $B_{x\,\mathrm{bias}} = -5$ G, $B_{y\,\mathrm{bias}} = -4.22$ G, and $B_{z\,\mathrm{bias}} = -1.87$ G.

Simulated maps of the magnetic-field strength distribution across the x-y plane located at an effective z distance above the magnetized film surface are shown in Figs. 1(d) and 1(e). Contour plots are shown for a finite magnetic lattice, Fig. 1(d) in the initial magnetic state formed by B_{ref} only and Fig. 1(e) with the application of external bias fields $B_{x\,\mathrm{bias}}$ and $B_{y\,\mathrm{bias}}$. Figures 2(a)–2(d) show the dependence of the magnetic-field gradient on α_h and α_s.

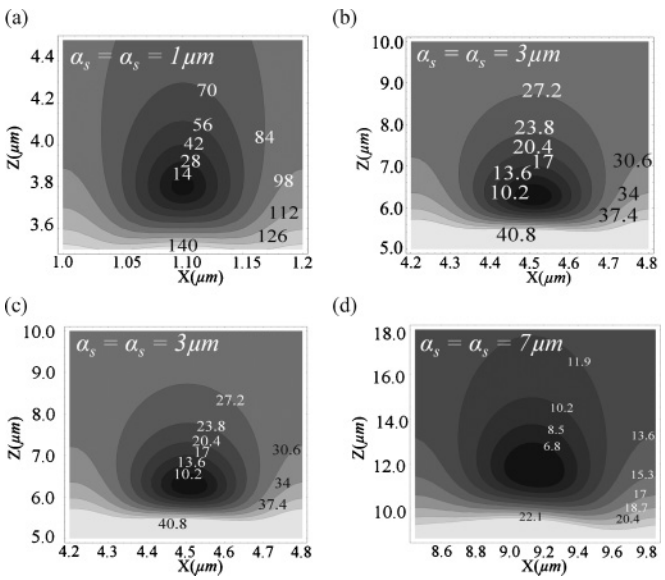

FIG. 2. (a)–(d) Contour plots of different magnetic-field gradients for different sizes of a single magnetic potential well simulated using different values of hole size α_h. The simulation is carried out using the parameters $M_z = 2.8$ kG, $\tau = 2$ μm, and with external bias fields $B_{x\,\mathrm{bias}} = B_{y\,\mathrm{bias}} = 1.5$ G. $\alpha_h = \alpha_s =$ (a) 1 μm, (b) 3 μm, (c) 5 μm, and (d) 7 μm.

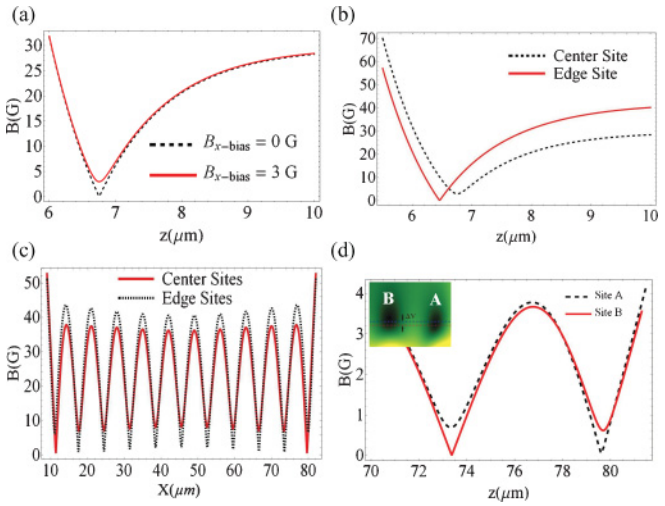

FIG. 3. (Color online) (a) Biased and unbiased magnetic-field minimum $B^z_{\min}$ along the z axis with $B_{x\,\mathrm{bias}} = 3$ G. (b) Magnetic-field minima along the z axis at the center and edge lattice sites. (c) Magnetic-field distribution along the x axis for an 11×11 2D magnetic lattice with $\alpha_s = \alpha_h = 3.5$ μm. (d) Two adjacent magnetic quantum wells at the lattice edge along the y axis separated by the magnetic barrier ΔB^y and having different values of nonzero local minima through a tilted (magnetic) potential. Simulation input parameters: $M_z = 2.8$ kG and $\tau = 2$ μm with no external bias fields applied in (b)–(d).

Figure 3(a) shows the location of the magnetic field nonzero local minimum $B^z_{\min}$ along the z axis at the distance $d_{\min}$ from the top of the hole. The results shown in Fig. 3(c) demonstrate the existence of nonzero local minima of the magnetic field along the x axis at the effective z distance.

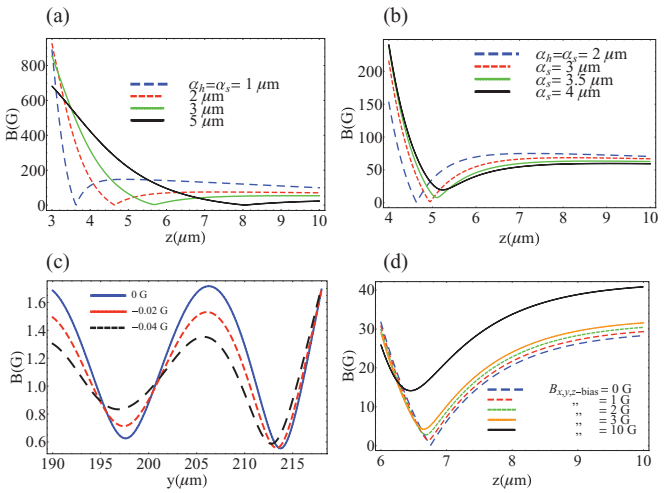

FIG. 4. (Color online) (a) Effect of changing the size of the holes, α_h, on the location of the magnetic-field local minima along the z axis at $d_{\min}$ above the holes of the thin film and (b) effect of changing the separation of the holes, α_s, across the x-y plane. (c) Simulation result of varying the barrier heights ΔB_y by applying a negative external $B_{z\,\mathrm{bias}}$ magnetic field and (d) $B_{x\,\mathrm{bias}}$, $B_{y\,\mathrm{bias}}$, and $B_{z\,\mathrm{bias}}$ effects on the gradient of the magnetic sites near the local minima along the z axis. A film thickness of $\tau = 2$ μm is used in the simulation results shown.

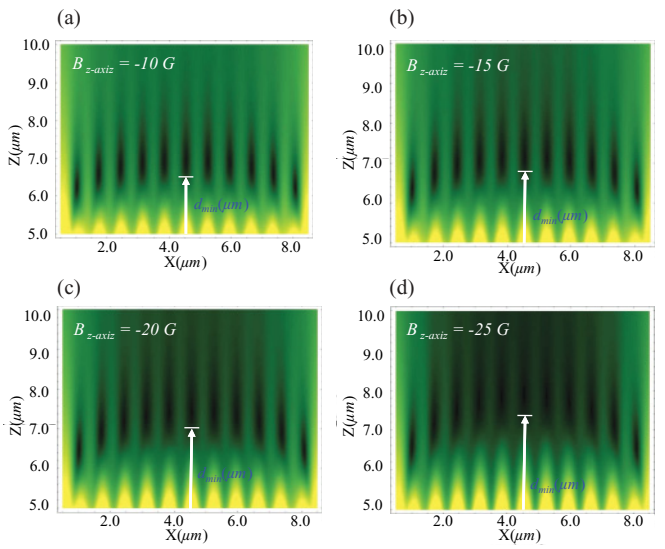

FIG. 5. (Color online) (a)–(d) Effect of applying a $B_{z\,\mathrm{bias}}$ field along the negative direction of the z axis on the magnetic barriers ΔB_y and ΔB_z and the nonzero magnetic local minima. Enhanced asymmetrical effect and $d_{\min}$ values are realized for different values of $B_{z\,\mathrm{bias}}$ field. Simulation input parameters: $n = 11$ sites, $\alpha_s = \alpha_h = 3.5$ μm, $M_z = 2.8$ kG, and $\tau = 2$ μm.

III. CHARACTERISTIC PARAMETERS OF THE ASYMMETRICAL TWO-DIMENSIONAL MAGNETIC LATTICE

We simulated the effect of changing the dimensions α_s and α_h on the characteristic parameters of the magnetic lattice, in particular the location of the nonzero local minima, their size, and the curvature of the magnetic field across each individual lattice site. A shallower or steeper magnetic potential can be realized by choosing suitable values of α_s and α_h. Increasing the separation α_s between the holes raises the value of the nonzero local minimum by several Gauss above zero, thereby eliminating Majorana spin flips. Also, large separation values, $\alpha_s \gtrsim 2.5$ μm, cause the magnetic minima to occur further from the surface, Figs. 4(a) and 4(b), which keep the cold atoms away from Casimir-Polder interactions.

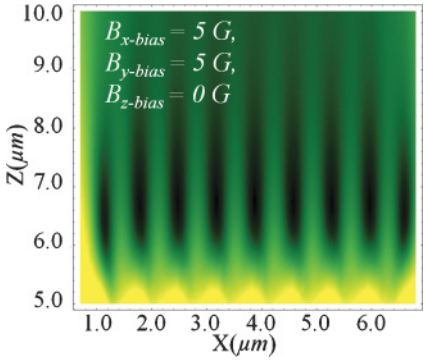

FIG. 6. (Color online) Applying external magnetic bias fields, $B_{x\,\mathrm{bias}} = B_{y\,\mathrm{bias}} = 5$ G, produces symmetrically distributed magnetic lattices sites with (almost) no offset of each lattice site. Simulation input parameters: $n = 9$, $\alpha_s = \alpha_h = 3.5$ μm, $M_z = 2.80$ kG, and $\tau = 2$ μm.

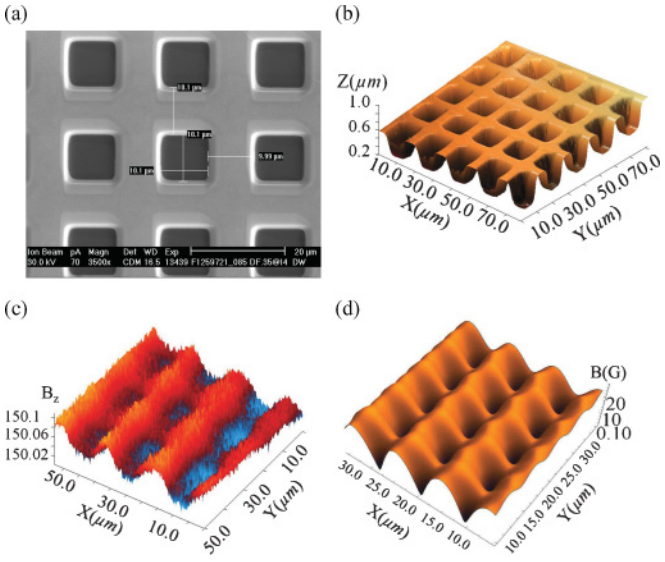

FIG. 7. (Color online) (a) Scanning-electron-microscope and (b) atomic-force microscope images of a fabricated 2D magnetic structure. (c) Magnetic field measured using the magnetic-force microscope and (d) simulation result of the *in situ* biased 2D magnetic lattice. Simulation and experimental input parameters: $\alpha_s = \alpha_h = 10\ \mu$m, $M_z \approx 2.80$ kG, and $\tau = 1\ \mu$m.

Another characteristic is identified for small n. There is a pronounced asymmetrical distribution of the magnetic local minima across the x-z and y-z planes; each two adjacent lattice sites, that is, site (i) and site $(i+1)$, are displaced along the z axis and differ from one another by a tilting potential ΔV_i^{i+1}, as shown in Fig. 3(d). We regard the magnetic lattice exhibiting an asymmetrical behavior as a *magnetic band gap structure* similar to the energy band gap structure in semiconductor devices which may allow the simulation of condensed matter systems using trapped degenerate quantum gases. Figures 4(a) and 4(b) summarize the simulation results of changing the hole size and the separating distance, and Figs. 4(c) and 4(d) show the effect of applying external magnetic-bias fields on the height of the magnetic barrier and the amount of potential tilt between each two adjacent lattice sites, along the y axis and z axis, respectively.

An asymmetrical magnetic lattice set at the reference magnetic field, B_{ref}, with no external bias fields, creates a magnetic confinement with B_{min} close to zero. This situation can be avoided by changing the separation α_s between holes to be larger than the hole size α_h. Another way of setting $B_{\text{min}} \neq 0$ is to apply external magnetic bias fields. Figure 5 shows the effect of applying different magnetic bias fields where we simulated an 11×11 asymmetrical magnetic lattice with $\alpha_h = \alpha_s = 3.5\ \mu$m. Moreover, applying external magnetic-bias fields, namely, $B_{x\ \text{bias}}$ and $B_{y\ \text{bias}}$, will maintain symmetrically distributed lattice sites across the x-z and y-z planes, as shown in Fig. 6. To realize tunneling of cold atoms, a relatively small separation ($\lesssim 2\ \mu$m) is necessary.

We have fabricated a magnetic lattice device by milling an $n \times n$ hole structure using a focused ion beam in a magnetic thin film (a 1-μm-thick film of $Bi_2Dy_1Fe_4Gd_1O_{12}$ material rf-sputtered onto a Si substrate). The detailed description of our experimental work will be reported elsewhere. Figures 7(a) and 7(b) show 2D and 3D images of the magnetic structure taken using a scanning electron microscope and an atomic-force microscope, respectively. The z component of the magnetic field of the asymmetrical magnetic lattice is measured using a magnetic-force microscope, as shown in Fig. 7(c).

IV. CONCLUSIONS

We have proposed a method of creating an asymmetrical 2D magnetic lattice suitable for trapping and confining ultracold atoms and quantum degenerate gases prepared in low-magnetic-field-seeking states. The proposed magnetic structure can be fabricated by milling an $n \times n$ array of square holes on the surface of permanent magnetic thin film. Simulation results have shown that it is possible to optimize the 2D magnetic lattice by choosing suitable values for the square hole size and their separating distance as well as by applying external magnetic bias fields. We have also proposed the possibility of creating discrete magnetic levels using the asymmetrical character in the distributed magnetic field in which we associate the discrete effect with a *magnetic band gap structure* similar to the energy band gap structure in semiconductor devices. This feature will make it possible, using magnetically trapped ultracold quantum gases, to simulate condensed-matter systems where many interesting problems can be investigated, such as exciton and biexciton formation, the Josephson effect [37], and long-range entanglement [38]. It is of a particular importance to highlight the simplicity of the method proposed in this article for achieving a 2D magnetic lattice using current state-of-the-art fabrication technologies. We have shown that applying external bias fields in the z direction can be used to control the potential barrier height and hence the tunneling process of the cold atoms between sites presenting the asymmetric 2D magnetic lattice as a promising candidate for processing quantum information, such as multipartite entanglement and qubit formation.

ACKNOWLEDGMENTS

We thank James Wang from the Centre for Atom Optics and Ultrafast Spectroscopy at Swinburne University in Melbourne for his help in measuring the surface magnetic field using the magnetic force microscope.

[1] I. Bloch, Nat. Phys. **1**, 23 (2005).
[2] O. Mandel, M. Greiner, A. Widera, T. Rom, T. W. Hänsch, and I. Bloch, Phys. Rev. Lett. **91**, 010407 (2003).
[3] B. Paredes, A. Widera, V. Murg, O. Mandel, S. Fölling, I. Cirac, G. V. Shlyapnikov, T. W. Hänsch, and I. Bloch, Nature (London) **429**, 277 (2004).
[4] Z. Hadzibabic, P. Krüger, M. Cheneau, B. Battelier, and J. Dalibard, Nature (London) **441**, 1118 (2006).
[5] I. Bloch, J. Dalibard, and W. Zwerger, Rev. Mod. Phys. **80**, 885 (2008).
[6] M. Greiner, O. Mandel, T. Esslinger, T. W. Hänsch, and I. Bloch, Nature (London) **415**, 39 (2002).

[7] R. Jördens, N. Strohmaier, K. Günter, H. Moritz, and T. Esslinger, Nature (London) **455**, 204 (2008).
[8] M. Köhl, H. Moritz, T. Stöferle, K. Gunter, and T. Esslinger, Phys. Rev. Lett. **94**, 080403 (2005).
[9] D. P. DiVincenzo, Fortschr. Phys. **48**, 771 (2000).
[10] O. Mandel, M. Greiner, A. Widera, T. Rom, T. W. Hänsch, and I. Bloch, Nature (London) **425**, 937 (2003).
[11] M. Riedel, P. Böhi, Y. Li, T. Hänsch, A. Sinatra, and P. Treutlein, Nature (London) **464**, 1170 (2010).
[12] J. Reichel, Appl. Phys. B **74**, 469 (2002).
[13] H. Ott, J. Fortágh, G. Schlotterbeck, A. Grossmann, and C. Zimmermann, Phys. Rev. Lett. **87**, 230401 (2001).
[14] W. Hänsel, P. Hommelhoff, T. W. Hänsch, and J. Reichel, Nature (London) **413**, 498 (2001).
[15] J. Fortágh and C. Zimmermann, Rev. Mod. Phys. **79**, 235 (2007).
[16] S. Ghanbari, T. D. Kieu, A. Sidorov, and P. Hannaford, J. Phys. B **39**, 847 (2006).
[17] S. Ghanbari, T. D. Kieu, and P. Hannaford, J. Phys. B **40**, 1283 (2007).
[18] M. Singh, M. Volk, A. Akulshin, A. Sidorov, R. McLean, and P. Hannaford, J. Phys. B **41**, 065301 (2008).
[19] J. Yin, W. Gao, J. Hu, and Y. Wang, Opt. Commun. **206**, 99 (2002).
[20] R. Gerritsma, S. Whitlock, T. Fernholz, T. Schlatter, J. A. Luigjes, J.-U. Thiele, J. Goedkoop, and R. Spreeuw, Phys. Rev. A **76**, 033408 (2007).
[21] T. Fernholz, R. Gerritsma, S. Whitlock, I. Barb, and R. J. C. Spreeuw, Phys. Rev. A **77**, 033409 (2008).
[22] I. Teper, Y.-J. Lin, and V. Vuletić, Phys. Rev. Lett. **97**, 023002 (2006).
[23] S. Whitlock, R. Gerritsma, T. Fernholz, and R. Spreeuw, New J. Phys. **11**, 023021 (2009).
[24] G. I. Opat, S. J. Wark, and A. Cimmino, Appl. Phys. B **54**, 396 (1992).
[25] T. M. Roach, H. Abele, M. G. Boshier, H. L. Grossman, K. P. Zetie, and E. A. Hinds, Phys. Rev. Lett. **75**, 629 (1995).
[26] A. I. Sidorov, R. J. McLean, W. J. Rowlands, D. C. Lau, J. E. Murphy, M. Walkiewicz, G. I. Opat, and P. Hannaford, Quantum Semiclass. Opt. **8**, 713 (1996).
[27] M. Singh, R. McLean, A. Sidorov, and P. Hannaford, Phys. Rev. A **79**, 053407 (2009).
[28] P. Treutlein, P. Hommelhoff, T. Steinmetz, T. W. Hänsch, and J. Reichel, Phys. Rev. Lett. **92**, 203005 (2004).
[29] D. Jaksch, J. I. Cirac, P. Zoller, S. L. Rolston, and D. M. Lukin, Phys. Rev. Lett. **85**, 2208 (2000).
[30] M. D. Lukin, M. Fleischhauer, R. Cote, L. M. Duan, D. Jaksch, J. I. Cirac, and P. Zoller, Phys. Rev. Lett. **87**, 037901 (2001).
[31] J. Cirac and P. Zoller, Nature (London) **404**, 579 (2000).
[32] R. Raussendorf and H. J. Briegel, Phys. Rev. Lett. **86**, 5188 (2001).
[33] D. Jaksha and P. Zoller, Ann. Phys. **315**, 52 (2005).
[34] S. Levy, E. Lahoud, I. Shomroni, and J. Steinhauer, Nature (London) **449**, 579 (2007).
[35] F. Cataliotti, S. Burger, P. M. C. Fort, F. Minardi, A. Trombettoni, A. Smerzi, and M. Inguscio, Science **293**, 843 (2001).
[36] W. M. Liu, W. B. Fan, W. M. Zheng, J. Q. Liang, and S. T. Chui, Phys. Rev. Lett. **88**, 170408 (2002).
[37] A. Abdelrahman, P. Hannaford, and K. Alameh, Opt. Express **17**, 24358 (2009).
[38] A. M. Abdelrahman, P. Hannaford, M. Vasiliev, and K. Alameh, in *Asia Communications and Photonics Conference and Exhibition*, Technical Digest (CD) (Optical Society of America, 2009), paper ThEE4.